

PRODUCTION OF HIGH PRESSURES WITH A MAGNETIC PINCH

by

Stephan Jay Bless

S. B., Massachusetts Institute of Technology

(1965)

SUBMITTED IN PARTIAL FULFILLMENT
OF THE REQUIREMENTS FOR THE
DEGREE OF MASTER OF
SCIENCE

at the
MASSACHUSETTS INSTITUTE OF
TECHNOLOGY
August, 1968

Signature of Author
Department of Geology and Geophysics, August 19, 1968

Certified by Thesis Supervisor

Accepted by
Chairman Departmental Committee
on Graduate Students



ABSTRACT

The effects of a fast capacitor discharge on iron, molybdenum, boron nitride, and quartz rods have been studied. Methods of energy transfer to the rods are discussed. Evidence is presented for production of the ϵ phase of iron, indicating a pressure of at least 130 kilobars.

TABLE OF CONTENTS

Abstract	2
1. Introduction	4
2. Related Research	
2.1 Exploding wires	6
2.2 Plasma confinement	7
3. Apparatus	9
4. Experimental Investigations	
4.1 Energy deposition	18
4.2 Experiments with a laser	23
4.3 Experiments with iron	24
4.4 Experiments with boron nitride	36
4.5 Experiments with quartz	40
5. Conclusions	44
6. Acknowledgements	44
7. References	45

1. INTRODUCTION

Modern high pressure research has been applied to a number of geophysical problems.^{8, 42, 54} Experiments with static pressure devices have been successful in duplicating the pressure and temperature regimes of the crust and upper mantle. In the lower mantle and core, pressures of 400 up to 3600 kilobars and temperatures of 1500 to 6000°K are encountered.^{8, 30} Static devices have been unable to produce pressures greater than 500 kb., and the pressure-temperature relation of the earth can only be reproduced to 100 Kilobars. Shock waves, however, are able to produce pressures as high as 5 megabars.²² Although the pressure-temperature relationship cannot be varied in shock waves, it is believed to be similar to that of the earth.⁴⁰ The disadvantages of shock compression are one-dimensional strain and short duration. A new means of pressure production, utilizing an electric pinch, is described in this paper. This method may be useful in supplementing shock wave data in the range of 100-500 Kilobars.

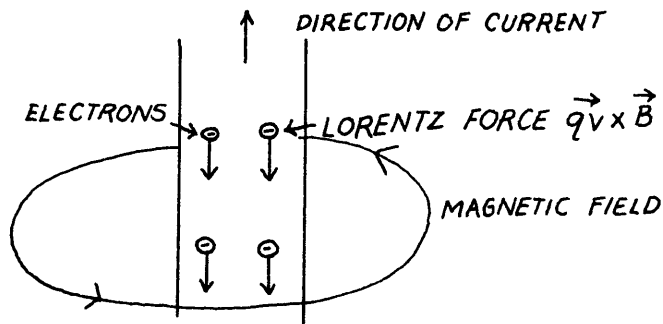


Fig. 1 - Geometry of pinch phenomenon.

The pinch effect results from the Lorentz force,

$$\vec{F} = q\vec{v} \times \vec{B},$$

acting on the current carrying electrons in a discharge. It can be seen from Fig. 1 that this force is inward. It results in a pressure which is proportional

to the square of the current

The experiments described in this paper were conducted with a capacitor discharge apparatus capable of producing currents exceeding 10^6 amperes. The work reported at this time is still incomplete; however, evidence for pinch pressure above 130 kilobars has been obtained.

2. RELATED RESEARCH

2.1 Exploding wires

For several years there has been a considerable interest in "exploding wire" phenomena^{14, 15, 16} because of engineering applications, such as explosive detonators,¹⁷ magnetic field compression,⁴⁵ and particle accelerators,⁹ and because of the theoretical challenges presented by interpretation of the observations.

In most exploding wire experiments, small diameter (a few mils) wires are vaporized by large current pulses (up to 10^6 amps) generated by capacitor discharges. These experiments probably produce pressures up to several hundred kilobars; however, pressures inside of an exploding wire have not been measured. Outward travelling symmetric stress waves of 30 kilobars²⁹ and temperatures of 10^5 °C³³ have been reported.

Schenk and Linhart have attempted to produce high magnetic fields by flux compression with an electrically imploded foil.⁴⁵ Usually, explosives are used for this purpose, and fields up to 2×10^6 gauss (corresponding to a pressure of 160 kilobars) have been produced.^{28, 38} The maximum field which Schenk and Linhart obtained was 10^5 gauss (corresponding to a pressure of 0.4 kilobars).

Most of the theoretical work treats problems peculiar to exploding wires. For this case, the wire is joule heated by a uniformly distributed current until melting occurs.⁶ Then a vaporization-expansion wave propagates into the wire at a speed of several hundred meters per second, converting the melted material to a dense metal vapor.⁵ Conduction ceases until the vapor expands enough for the residual capacitor voltage to break down the gap between the electrodes; conduction, in this stage, is through the outer regions of the plasma sheath surrounding the wire.³⁶ Confinement thus has an important effect on the later discharge.⁴¹

There is one fundamental difference between exploding wires and the rods used in our experiments. The skin depth for current penetration is approximately

$$s = \sqrt{\rho / \pi \nu \mu_0}$$

Here, ρ = resistivity, $\mu_0 = 4 \pi \times 10^{-7}$ h/m, ν = frequency, and d = wire diameter. For exploding wire work $s \geq d$, whereas in our experiments $s \ll d$.

2.2 Plasma Confinement

Many attempts have been made to confine hot plasmas with pinch pressure. At one time it was believed that a linear pinch device might be successful in containing a nuclear fusion reaction,⁴⁴ but it is now thought that such pinches are intrinsically too unstable.⁵⁰

In the typical plasma pinch experiment, the discharge is through a gas, the pinch is stabilized by an axial magnetic field, the current diameter is of the order of centimeters, and the exterior pressure, $B^2 / 2 \mu_0$, is not large. The experiments of Komelkov provide a feeling for the scale involved.³⁶ In these experiments, a 130 μ f capacitor bank producing peak currents of 9×10^5 amperes was used. Typical plasma motions, recorded with a Kerr-cell camera, were around 5×10^6 cm/sec. Figure 2 shows the course of a discharge observed by Komelkov.

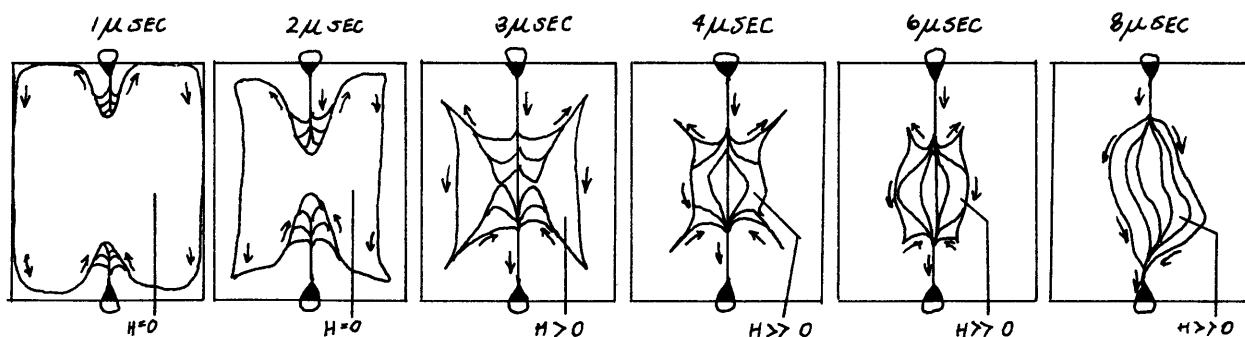


Fig. 2 - Plasma motions in a discharge. Initial pressure 1 mm Hg. H is the magnetic field. (from reference 36)

The smallest current cords which Komelkov observed were around 1 cm

diameter. Assuming that the maximum current went through this cord, the corresponding pressure (our calculation) was less than 100 atm. Komelkov estimates the maximum pressure to have been 10^9 dynes/cm² (1000 atm) at the center of the discharge.

Further research by Folkierski and Lathane²⁷ has shown the existence of converging shock waves in such discharges. Koppendorfer³⁷ has shown that only a conducting gas is compressed by magnetic pressure.

More recently, attempts at plasma confinement have concentrated on toroidal pinches lasting for many milliseconds. These experiments bear very little relation to phenomena likely to occur with our apparatus.

3. APPARATUS

The energy bank consists of eight $15\mu\text{f}$, 3000 joule, 20 kilovolt Tobe Deutschmann Laboratories low inductance capacitors, arranged symmetrically about octagonal aluminum plates, as shown in figure 3.

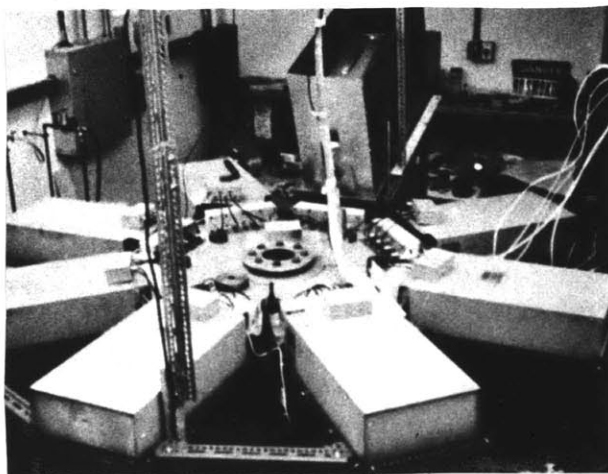


Fig. 3 - Photograph of the capacitors and aluminum plates.

Each capacitor is triggered separately by a sparkgap. In early experiments frequent prefiring presented a problem, but this has been largely eliminated by careful attention to the condition of the gaps. Simultaneity of the discharges, however, is only achieved for capacitor voltages above 16 kilovolts.

The aluminum plates are $3/8$ inch thick, and are separated by 0.060 inches of mylar insulation. The sample holder assembly is inserted in the center of the plates; figure 4 is a diagram of this assembly. The inside diameter of the boron nitride cylinder could be varied. In most of the experiments a 5mm diameter hole (not shown in the figure) passed through the sample holder; the hole was 2mm off center and inclined at 20° . This hole was originally drilled to enable entry and exit of a laser beam; it was retained for later experiments to allow hot gases to escape. Indeed, sparks issuing from it once started a fire in some empty boxes

10 feet away.

Hardened steel slugs are inserted in the phenolic blocks behind the electrodes in order to prevent erosion of the blocks by the blasts. The phenolic blocks are pressed together by a pair of heavy anvils. The current path is through the aluminum plates, the copper annuluses, the .010 inch copper disc electrodes, and the sample. After each shot metal deposits have to be filed off the steel inserts, and the phenolic blocks have to be replaced or repaired after four or five shots. Especially violent explosions (resulting from high energy density or loose assembly) often cause severe damage to all parts of the sample chamber and mylar insulation. For this reason, the chamber and center plate sections were designed for easy disassembly and replacement.

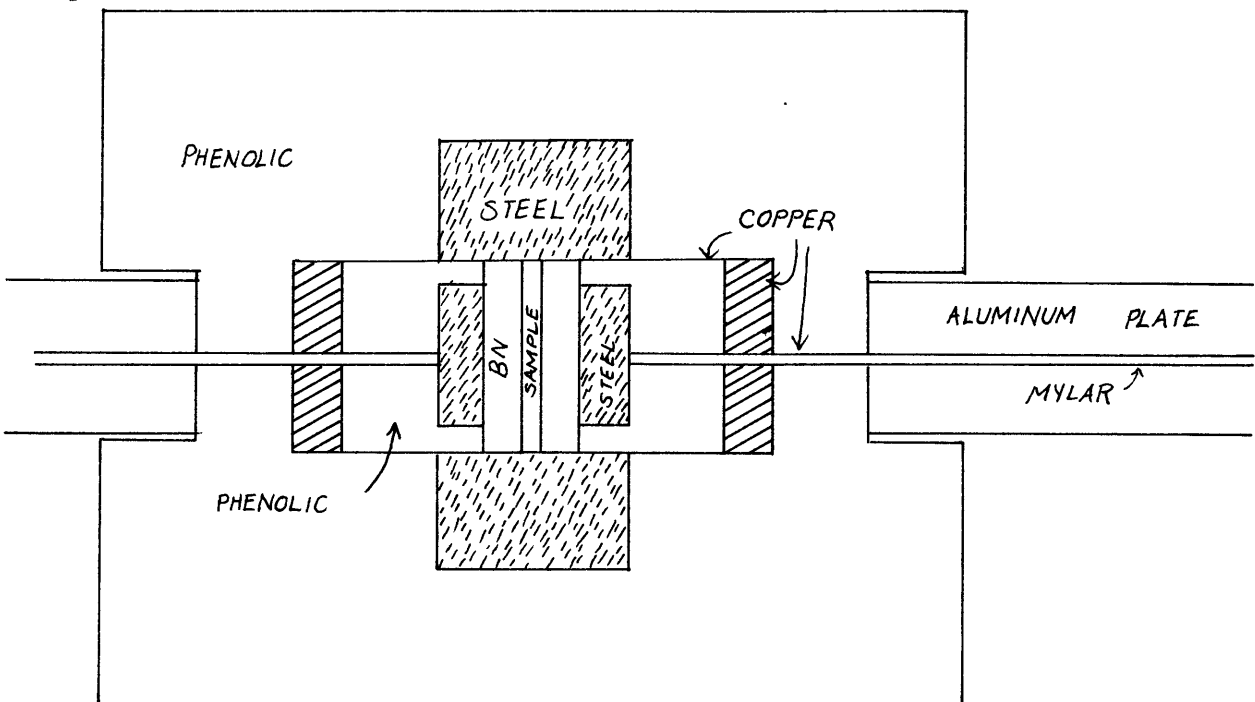


Fig. 4 - Sample chamber

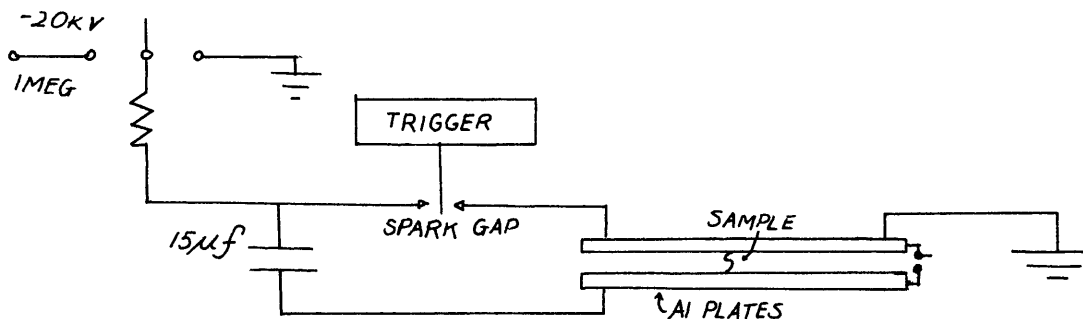


Fig. 5 - A capacitor circuit

The voltage between the plates was monitored with a Science Accessories Corporation model 003 high voltage probe. The probe signals were recorded with Tektronix models 547 and 555 oscilloscopes. Figure 6 is a reproduction of a typical signal. The voltage across the individual capacitors could be independently measured with a 400 megaohm voltage divider constructed for that purpose.

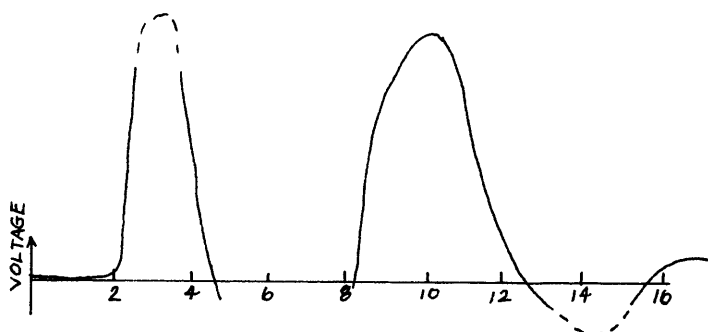


Fig. 6 - Typical oscillograph; copper coated 4mm BN rod. 8 capacitors, 19.8 kV, 2 μ sec/div. The dotted portions of the waveform could not be read on the photograph.

Copper coils were inserted between the mylar sheets. For a symmetric current distribution, the voltage induced around the loops was proportional to $\frac{di}{dt}$.

However, only in the few experiments in which all eight capacitors were fired could the signal from the loops be interpreted.

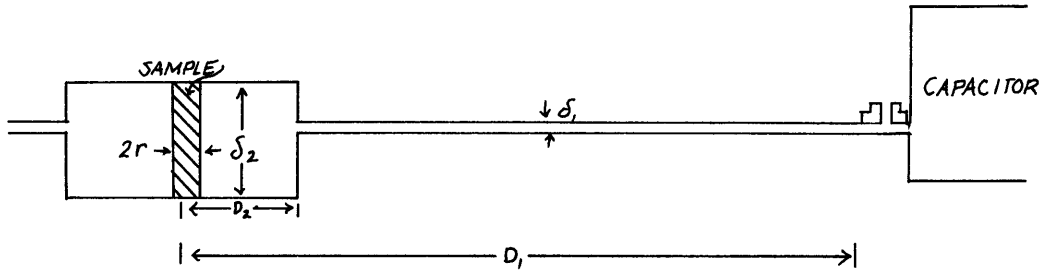


Fig. 7 - Geometry for inductance calculation.

The inductance of the sample and aluminum plates can be calculated. Figure 7 illustrates the geometry and defines the symbols used in the calculation.

We may write,

$$L_{\ell} = \frac{\Phi}{I}, \quad B = \frac{\mu_0 i}{2\pi r}, \quad \text{and} \quad \Phi = \iint \vec{B} \cdot d\vec{S}.$$

Thus, (1)

$$L_{\ell} = \frac{\mu_0 \delta}{2\pi} \ln \frac{D_1}{r} \equiv L_p + L_s$$

We first calculate the contribution from the aluminum plates, which is independent of the sample diameter:

$$L_p = \frac{\mu_0 \delta_1}{2\pi} \ln \frac{D_1}{D_2} = .747 \text{ nanohenries.} \quad (2)$$

The contribution from the sample chamber is

$$L_s = \frac{\mu_0 \delta_2}{2\pi} \ln \frac{D_2}{r} = 12.9 \text{ nh for a 4mm diameter sample.} \quad (3)$$

Therefore, the total inductance of the sample and plates is 13.6 nh for a 4mm diameter sample. The resistance of the rod is small compared to this: let ρ be the resistivity, ℓ the length, s the skin depth, T the discharge period, and r the radius. Then

$$R_s = \frac{\rho \ell}{\pi s (r - s)} \quad ; \quad s = \sqrt{\frac{\rho T}{\pi \mu_0}} \quad (4)$$

For $r = 2\text{mm}$ and $T = 8 \times 10^{-6}$, equations (4) give $R_s = .75 \times 10^{-3}$ ohm. This should be compared with ωL_ℓ which is $\sim 10.7 \times 10^{-3}$ ohm. Also, for this case, $R/L = .055 \times 10^6$.

The inductance of a spark gap is calculated to be 6.7 nh. The rated inductance of a capacitor is 5 nh. This makes a total source inductance, L_0 , of 11.7 nh. The uncertainty in this figure is about 20% because the current distribution in the spark gaps is not well known and the capacitor inductance rating is approximate.

In an RLC discharge,

$$I = e^{j\omega t},$$

and

$$\begin{aligned} \omega &= \omega_r + j\omega_i; \\ \omega_i &= R/2L, \quad \omega_r = \sqrt{\frac{1}{LC} - \frac{R^2}{4L^2}} \end{aligned} \quad (5)$$

The period of an oscillatory discharge in our system should, thus, be given by

$$\begin{aligned} T &= \frac{2\pi}{\sqrt{\frac{1}{LC} - \frac{R^2}{4L^2}}} \approx 2\pi\sqrt{LC} \\ &= 2\pi\sqrt{C_0 (L_0 + NL)}, \end{aligned} \quad (6)$$

where $C_0 = 15 \mu\text{f}$, $L_0 = 11.7 \text{ nh}$, L_ℓ is given by equations (1) through (3), and

N is the number of capacitors fired. Values of T, calculated from equation (6), are given in Table 1.

Table 1 - Values of the discharge time T, calculated from equation (6), for a 4mm diameter sample.

N	T (μsec)
1	3.86
2	4.80
3	5.56
4	6.28
5	6.88
6	7.42
7	7.95
8	8.45

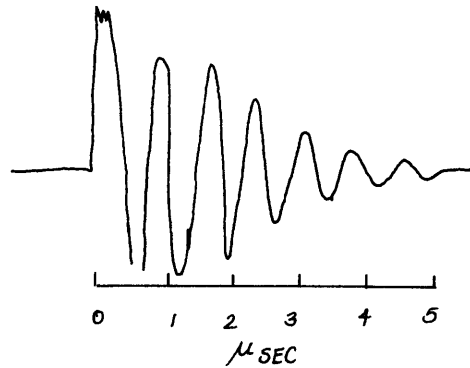


Fig. 8 - Oscilloscope of discharge through 4mm dia. Fe rod. 1 capacitor, 14.3 kV.

The discharge period measured on the oscilloscope was often two or three times less than the value predicted by equation (6). Figure 8 shows a discharge through a 4mm iron rod with only one capacitor. In this experiment, the rod was not at all damaged. Applying equation (5) to the first portion of the oscilloscope, we can calculate $R/L \cong .66 \times 10^6$, and $L \cong 1 \text{ nh}$. Figure 9 shows a discharge at higher

energies in which the rod was destroyed. Even in this case, $T \approx 1.5 \mu\text{sec}$, from which $L \approx T^2/4\pi^2 C \approx 6\text{nh}$.

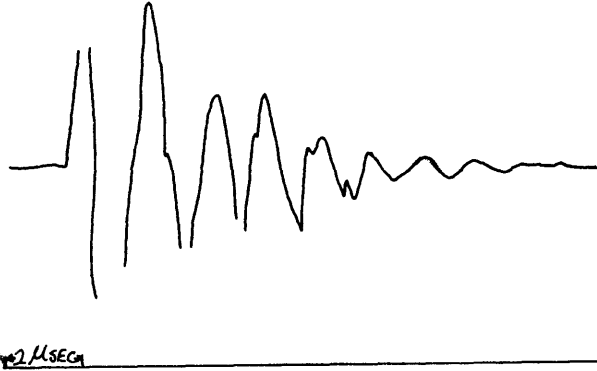


Fig. 9 - 4mm hollow Fe rod. 6 capacitors at 16 kV. (Missing sections of the curve did not register on the original photograph.)

The discrepancy between observed and predicted values of T is significant. An error of the required magnitude in the calculated inductance seems unlikely. Since several oscilloscopes were used at various times, scope miscalibration is also unlikely. Oscillograph traces from both the voltage probe and copper loops indicated similar periods. It is possible that either the probes or the oscilloscopes responded to a high frequency parasitic source; fortunately, the analysis of the results does not depend critically on exact knowledge of the voltage waveform.

The charge stored in the capacitors is

$$Q = CV = NC_0 V.$$

Therefore, the maximum charge in the capacitor bank is:

$$\begin{aligned} Q_{\text{max}} &= 8 \times 15 \times 10^{-6} \times 20 \times 10^3 \\ &= 2.4 \text{ coulombs,} \end{aligned}$$

and the stored energy is

$$\begin{aligned} U &= \frac{1}{2} NC_0 V^2. \\ U_{\text{max}} &= 24,000 \text{ joules} \\ &= 5760 \text{ calories} = 18000 \text{ ft-lbs.} \end{aligned}$$

The current, $I(t)$, flowing through the circuit is

$$I(t) = \frac{dQ}{dt} = -\omega Q_0 \sin \omega t.$$

$$I_{\text{average}} = \frac{1}{\sqrt{2}} \omega Q_0 = \frac{1}{\sqrt{2}} \frac{2\pi}{T} Q_0.$$

$$I_{\text{max}} = \frac{2\pi}{T} N C_0 V.$$

The uncertainties in the discharge period make calculation of the current difficult.

The highest current that has been recorded is 5×10^6 amperes. The oscillograph for that shot is reproduced in figure 10. However, the value of T from Table 2, corresponding to $N = 6$, gives a current of 1.2×10^6 ampere for this shot.

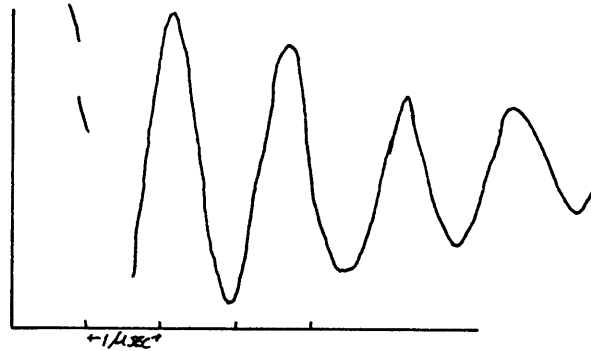


Fig. 10 - 4mm dia. iron rod, initial temp. 80°K . 6 capacitors, 16.2 kV.
(Missing portions of the curve in this reproduction were too light on the actual photograph to trace with confidence.)

The magnetic field is calculated from Ampere's Law.

$$2\pi r B = \mu_0 I,$$

$$B = \frac{\mu_0 I}{2\pi r} = \frac{4 \times 10^{-7}}{d} I \quad (\text{MKS}).$$

In order to minimize the current diameter, many of the rods were tightly confined in boron nitride sleeve cylinders. Figure 10 is a record of such a shot; the field calculated from the measured period is 5×10^6 gauss, but the predicted field is 1.2×10^6 gauss.

The pinch pressure associated with the magnetic field is

$$P = \frac{B^2}{2\mu_0} = \frac{I^2 \mu_0}{8\pi r^2} \cdot$$

$$P_{\max} = \frac{2\mu_0 N^2 C_0 V^2}{\pi T^2 d^2} \cdot$$

For $C_0 = 15\mu\text{f}$, $d = \tilde{d}$ mm, $V = \tilde{V}$ kV, and $T = \tilde{T}\mu$ sec, P_{\max} becomes:

$$P_{\max} = 5.66 \frac{N^2 \tilde{V}^2}{\tilde{d}^2 \tilde{T}^2} \text{ kilobars.} \quad (7)$$

For example, $\tilde{T} = 8$, $N = 8$, $\tilde{V} = 20$, and $\tilde{d} = 3$ gives $P_{\max} = 252$ kilobars.

The pressure calculated from the oscillograph shown in figure 10 is 1030 kilobars.

Unfortunately, that rod was completely vaporized. Figure 11 shows the predicted pressure obtainable at 20 kV for 4mm and 2mm diameter rods.

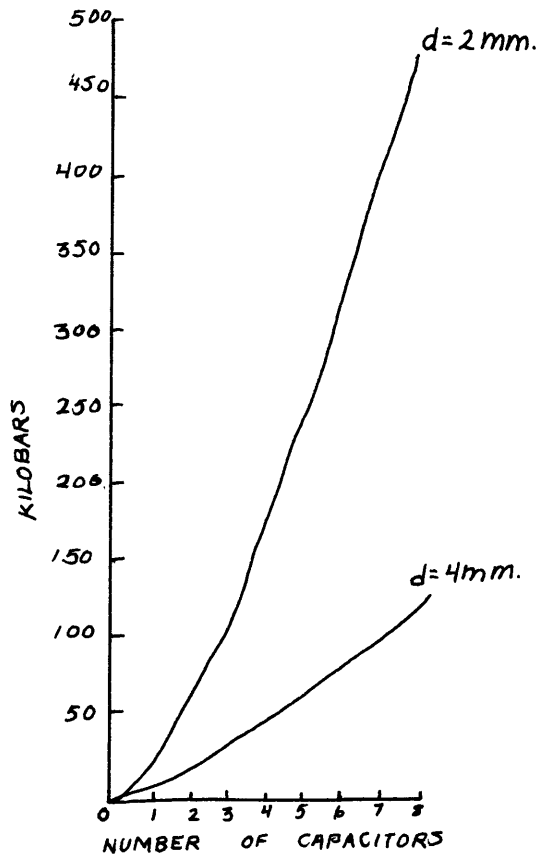


Figure 11 - Maximum pressure possible in 2mm and 4mm diameter rods. Calculated from equations (6) and (7) and table 2.

4. EXPERIMENTAL INVESTIGATIONS

The principal objective of the experimental investigations was to determine the applicability of the Z-pinch device to high pressure research. To this end, five groups of experiments have been carried out:

a) Energy studies - the first series of experiments were performed to discover what factors determine whether a given rod is destroyed in a discharge. These early experiments can be combined with data from later ones to indicate how energy is deposited in the sample.

b) Laser interaction - a few experiments were performed in order to observe the interaction of a laser beam with the plasma surrounding the rod.

c) High pressure effects in iron - attempts were made to produce the 130 kbar transition in iron. These efforts have apparently been successful.

d) Experiments with boron nitride - attempts were made to produce the high pressure phases of this substance. No evidence of success has been obtained.

e) Experiments with quartz - attempts were made to produce high pressure and/or high temperature phases of quartz. The results have been ambiguous.

These investigations are described in detail in the remainder of this section.

4.1 Energy deposition

The first experiments, under the supervision of Professor Francis Bitter, studied the effect of the discharge on various diameter molybdenum and stainless steel rods. At that time, only four capacitors were available, limiting the energy to 12,000 joules (2870 calories).

One immediately obvious fact was the confinement of the current to the skin depth, which is roughly given by the usual expression $s = \sqrt{\frac{\rho}{\pi \mu \nu}}$. Figure 12 is a photomicrograph of a molybdenum rod, showing regions of undisturbed metal, recrystallized melt, and recrystallized vapor. The oval-shaped intrusion is

copper colored; in the experiment, the nearest copper electrode was 1/2 inch away from where the picture was taken.

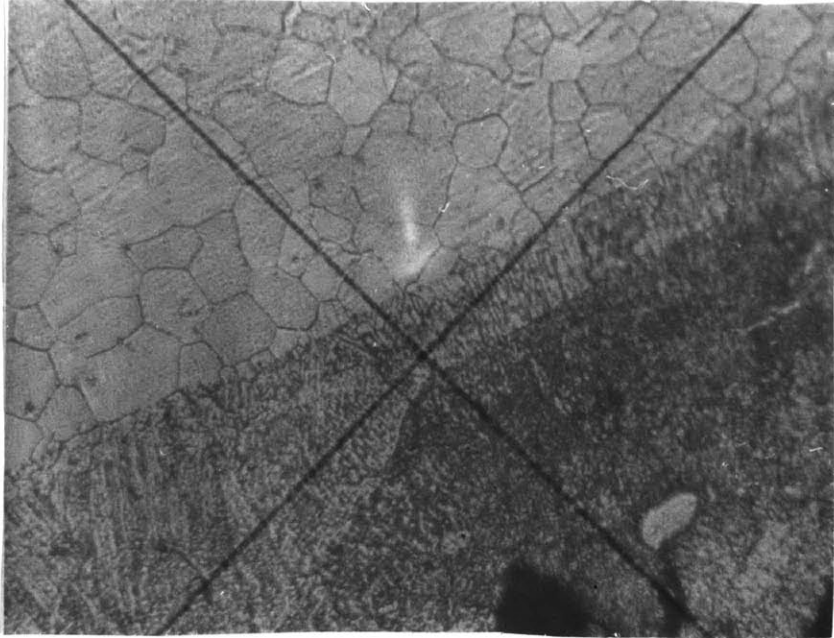


Fig. 12 - Photomicrograph of a 5.1mm diameter Mo rod, after a discharge with 4 capacitors at 20 kilovolts. 250X

Only six sizes of rods were used. These samples were loosely confined in 7.15 mm diameter boron nitride cylinders; there were no holes in the sample chamber. Figure 13 shows how the discharge affected the rods. The experimental parameter used in figure 13 is energy/unit volume. The importance of this quantity in determining the effect of the discharge is demonstrated in figure 14.

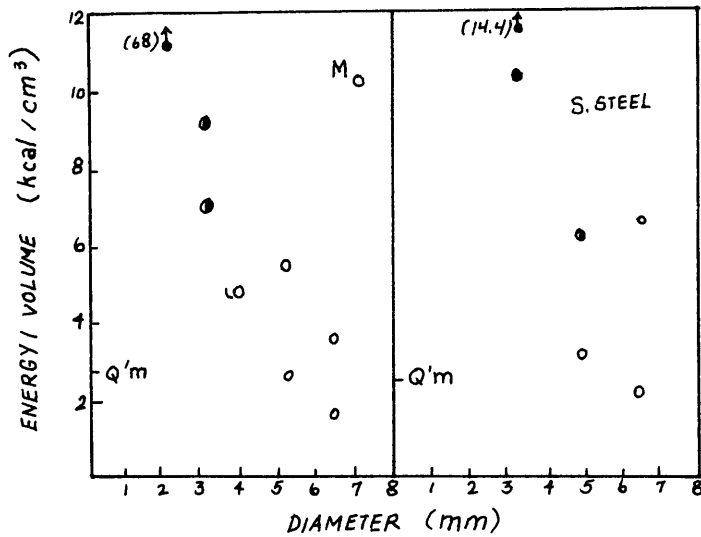


Fig. 13 - Effect of the discharge on molybdenum and stainless steel rods.

Open circles represent very little damage, half open circles are badly damaged but not broken, filled circles represent complete destruction.

Q'_m is the energy required to melt the rods (calculated on page 23).

Fig. 14 - Effect on 4mm dia. annealed, tightly confined Armco iron rods. The energies required to melt and vaporize the rod are shown.

Fig. 15 - Effects on all 4mm diameter iron rods. Group 1 were neither annealed nor confined. Group 2 are those shown in figure 14.

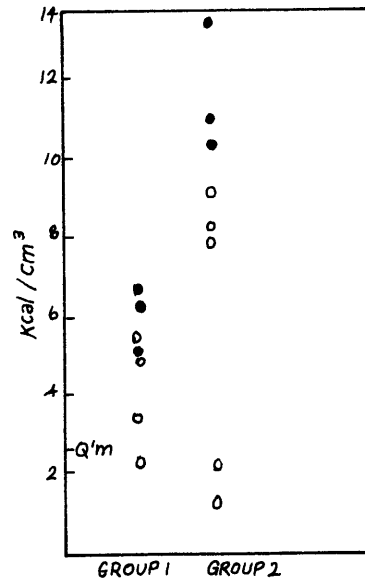
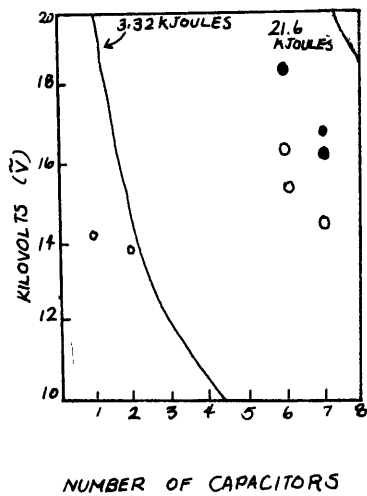


Figure 15 shows the results obtained with all of the 4mm rods which have been fired. The rods in Group 1 disintegrated at considerably lower energy levels than those in Group 2.

The energies required to melt and vaporize molybdenum and iron rods are calculated as follows:

For molybdenum:

melting point = 2890°K

$H(1, 2890) - H(s, 293) = 26,940$ calories (ref. 34)

Therefore $Q'_m = 2.69 \times 10^4 \text{ cal/mole} \times (95.95 \text{ gm/mole})^{-1} \times 10.22 \text{ gm/cc}$
 $= 2.87$ kilocalories/cc = 12.0 kilojoules/cc.

For iron (and stainless steel)

melting point = 1812°K

$H(1, 1812) - H(s, 293) = 17.68$ kcal/mole (ref. 34)

Therefore $Q'_m = 17.68 \times 10^3 \text{ cal/mole} \times (55.85 \text{ gm/mole})^{-1} \times 7.87 \text{ gm/cc}$
 $= 2.49$ kcal/cc = 10.4 kj/cc = 3.32 kj/4mm dia rod.

boiling point = 3000°K

heat of fusion at 1812° = 1598 cal/gm = 12.63 kcal/cc (ref. 38)

$H(g, 3000) - H(g, 1812) = 7000$ cal/mole = .975 kcal/cc (ref. 24)

Therefore $Q'_v = \text{heat required to vaporize} = 16.12$ kcal/cc = 67.5 kj/cc
 $= 21.6$ kj/4mm dia rod.

Consideration of these calculations and the observations recorded in figure 15 seems to justify the following conclusions:

- a) Unless the rod is broken, only a small portion of the energy in the capacitor bank is deposited in it.
- b) Complete vaporization of 4mm rods is energetically impossible, even in cases where the rod was completely destroyed.
- c) The effect of confinement on a rod is to increase the energy required to destroy it.

The first of these conclusions can be explained theoretically by adopting a model in which the current progressively melts outer layers of the rod and moves inward. We let

$$Z_1(r) = R_s + \omega(L_s + L_p)$$

equal the impedance for conduction through a solid rod of radius r . L_p , L_s , and R_s are given by equations 2, 3, and 4:

$$Z_1(r) = \frac{\rho \ell}{\pi s(2r - s)} + \omega L_s(r) + \omega L_p.$$

The impedance for conduction through a melted cylindrical shell of outer radius r_o and inner radius r is

$$z_2(r) = \begin{cases} \frac{\rho_m \ell}{\pi s(2r_o - s)} + \omega L_s(r_o) + \omega L_p & \text{for } r_o - r > s \\ \frac{\rho_m \ell}{\pi(r_o^2 - r^2)} + \omega L_s(r_o) + \omega L_p & \text{for } r_o - r < s. \end{cases} \quad (8)$$

In order to evaluate (8), the resistivity for liquid iron at high temperatures must be known. F.D. Bennet obtained the resistivity for an exploding copper wire as a function of specific energy: ρ_m did not increase much above 150×10^{-8} ohm-m until vaporization began.⁶ Therefore, the use of the handbook value of the resistivity of liquid iron, 139×10^{-8} ohm-m (ref 39), seems justified in this case.

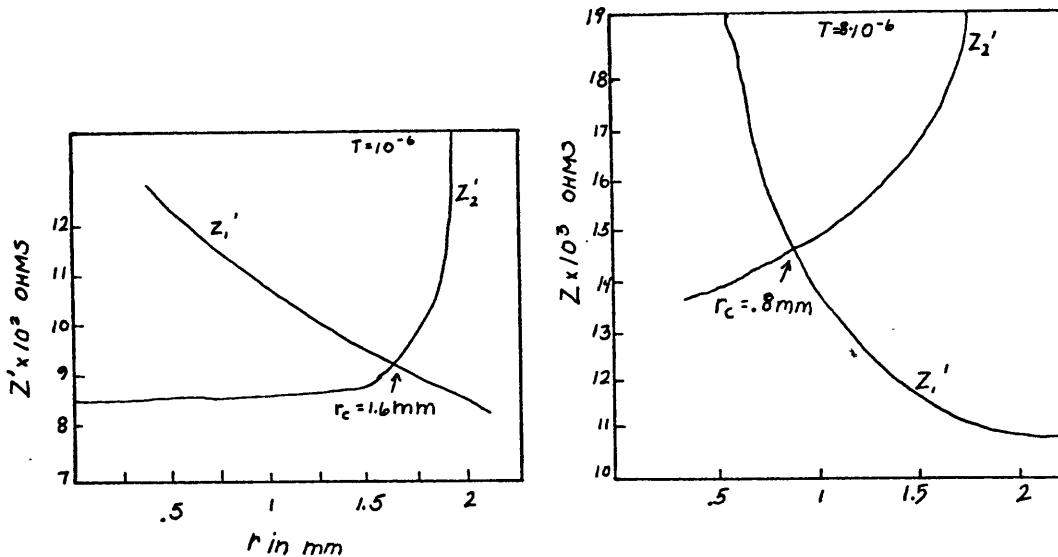


Fig. 16 - Solution of $Z_1(r) = Z_2(r)$. $Z' = Z - \omega L_p$ is plotted.

Figure 16 represents a graphic solution of the equation $Z_1(r) = Z_2(r)$ for two different values of T . In both cases the solution, r_c , is slightly underestimated because the increase in the resistivity of solid iron with temperature has not

been taken into account. Since r_c is appreciably less than two, it has been demonstrated that the current will be shunted by the outer melted material after only a small penetration into the solid rod.

The explanation for conclusions (b) and (c) could be that instabilities in the plasma sheath formed around the rod are chiefly responsible for its destruction. When the rods are confined, the plasma is suppressed. Destruction occurs if the scale of plasma instabilities reaches a critical size and can overcome the strength of the rod. Several exploding wire observations support this hypothesis.^{25, 26}

4.2 Preliminary experiments with a laser

In a few experiments, the dense plasma which results when a rod is vaporized was studied with an helium-neon laser. For this purpose, a 5mm hole was drilled through the sample chamber shown in figure 4; the hole was 2mm off center and inclined at a 20° angle. The intensity of light emerging from the sample chamber was measured with a photomultiplier tube.

Fig. 17 - Oscillograph of laser experiment. Upper trace is the photomultiplier voltage, lower trace is the voltage probe.

.062 inch steel rod fired with 1 capacitor at 14 kV.

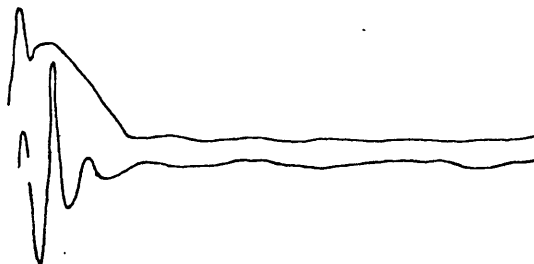


Figure 17 shows the oscillograph record from one of these shots. The attenuation of the laser signal is caused by the expanding plasma column. The plateaus in the photomultiplier output at current maxima suggest that the expansion of the plasma is retarded by pinch pressure.

4.3 Experiments with iron

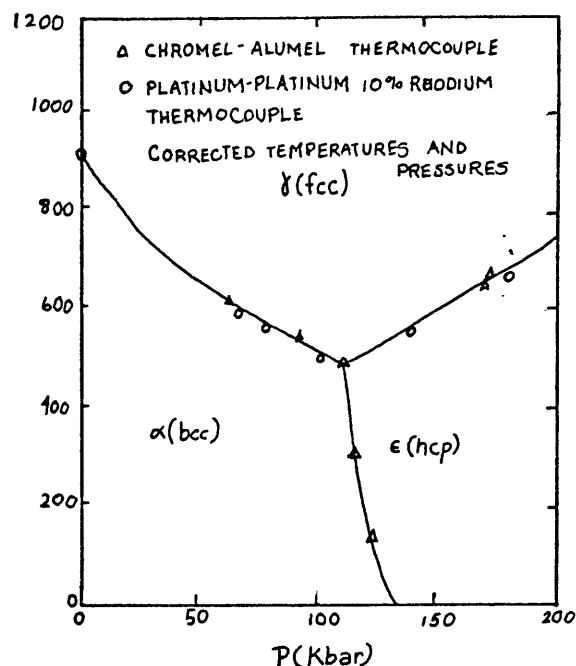


Fig. 18 - Phase diagram of iron. ¹² (from ref. 12)

Figure 18 shows the phase diagram for iron. The three principal phases are labeled α (body centered cubic), γ (face centered cubic), and ϵ (hexagonal closest packed). The ϵ phase was first produced in shock experiments, and was the classic example of a 2-wave structure caused by a phase transition.⁴ The temperature variation of the transition has been followed by Johnson *et. al.* dynamically³² and by Drickamer²⁴ and Bundy¹² statically.

A number of metallographic studies have been done on the effects of shock waves in iron.^{32, 47, 48} Figures 19 and 20 illustrate the difference in appearance between stock annealed iron and iron which has been shocked above 130 kilobars. The lines crossing the ferrite grains are mechanical twins, or Neumann bands. These are characteristically produced by shear in iron; however, no other process produces them in such quantity as shock loading above 130 kilobars.



Fig. 19 - Microstructure of untransformed iron. 192X (ref. 32)

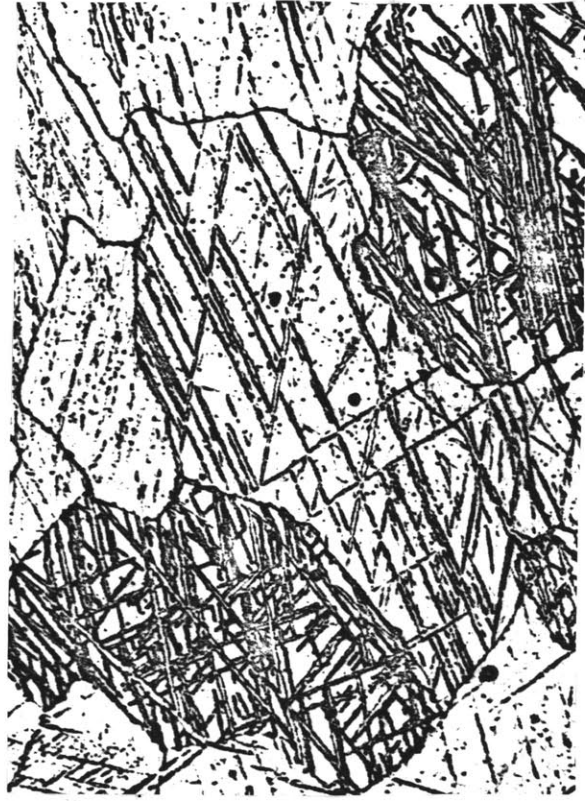


Fig 20 - Microstructure of iron which has been shocked through the ϵ stability region. 192X (ref. 32)

The angular distribution of the twin markings make it clear that they are associated with the shock compression (and not the shock rarefaction). Smith found that the angular distribution of twins has a maximum at 20° angle to the shock direction.⁴⁷

The effect of shock loading above 130 kilobars can be most dramatically seen when the rarefaction wave from a free surface cancels the compression wave, as illustrated in figures 21 and 22. A hardness increase of 10% occurs across this interface, as shown in figure 23.

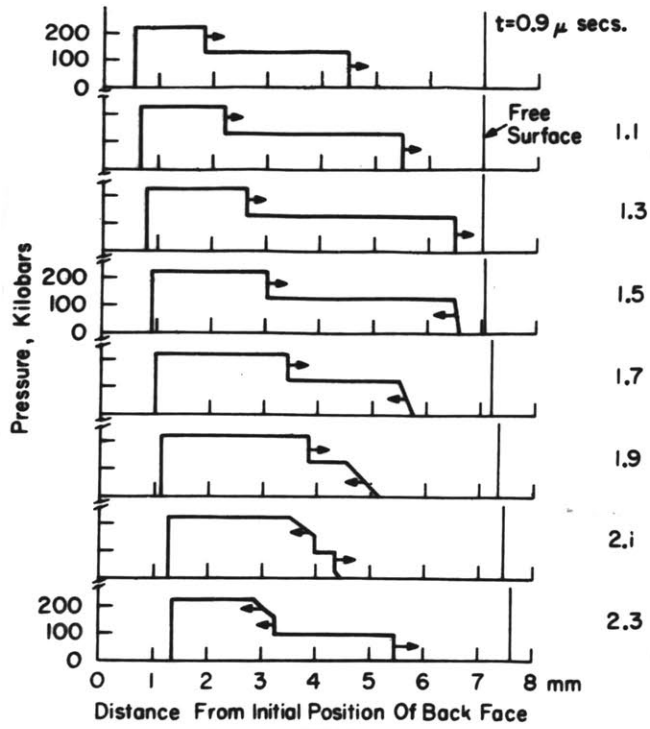


Fig. 21 - Shock reflection from a free surface. (ref. 47)

Fig. 22 - Resulting discontinuity in microstructure. Armco iron. 100X (ref. 47)

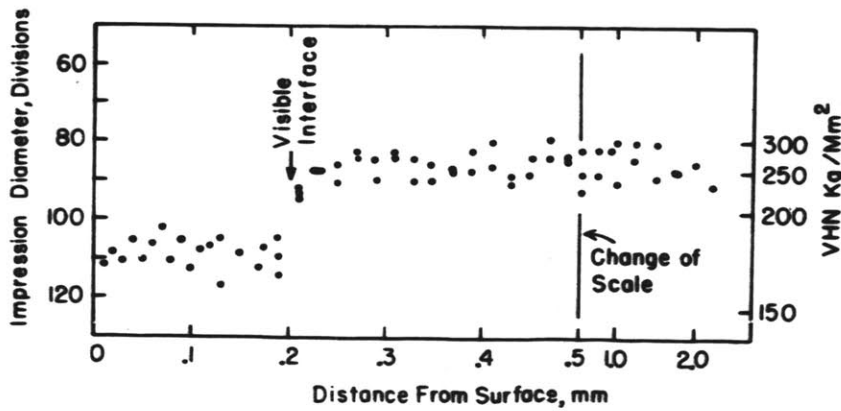
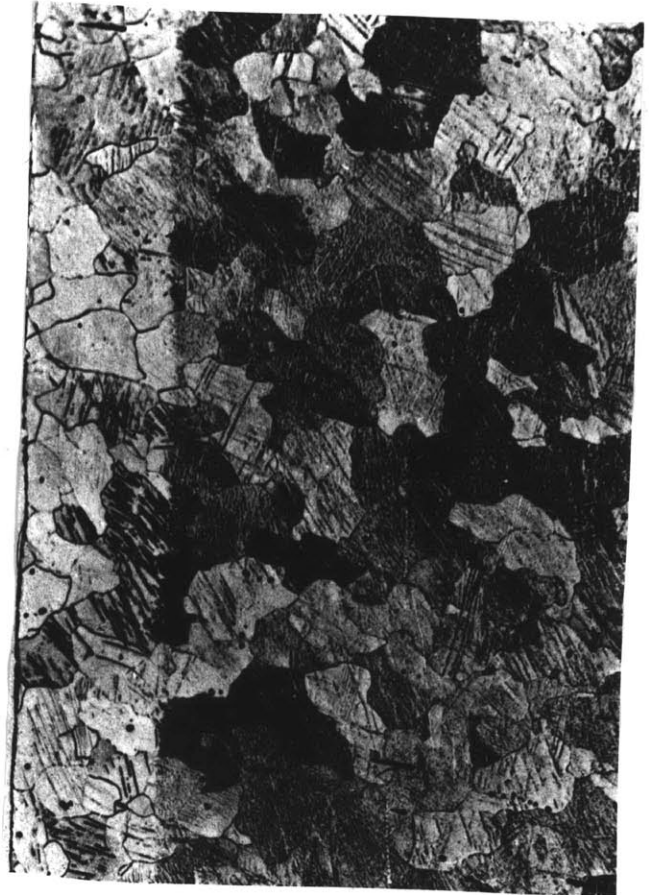


Fig. 23 - Resulting discontinuity in microhardness. (ref. 47)

In our preliminary experiments, seven 4mm diameter Armco iron rods were fired at various combinations of voltage and capacitance. The choice of 4mm for the diameter was unfortunate, in view of the predicted pressures of figure 11. However, examination of the figure shows that only small current penetration will enable pressures greatly exceeding 130 kilobars to be produced; such current penetration is predicted by the solution of equation (9).

It was the procedure in these and subsequent experiments to subject the rods to the largest possible energy without causing complete destruction; the remaining portions were then analysed for metallographic evidence of a phase transition. The maximum energy which the rods could absorb without disintegrating^e was found to be 11.5 kilojoules. Figure 24 illustrates these observations.

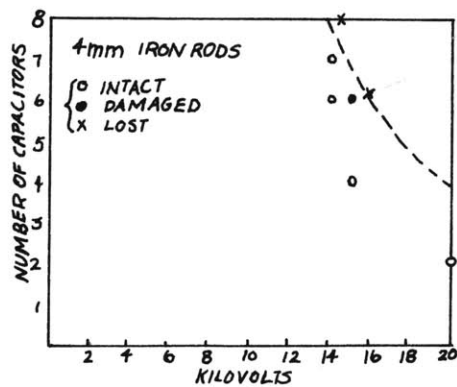


Fig. 24 - Response of 4mm Armco rods. Loose confinement; no holes. Circles have same meaning as in fig. 13.

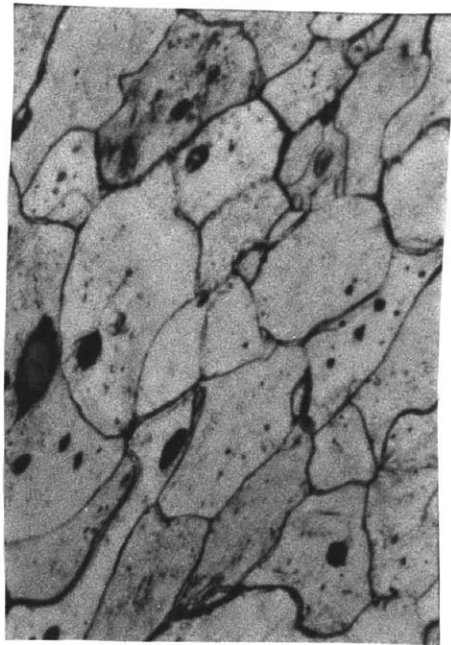


Fig. 25 - Stock Armco iron. 200X

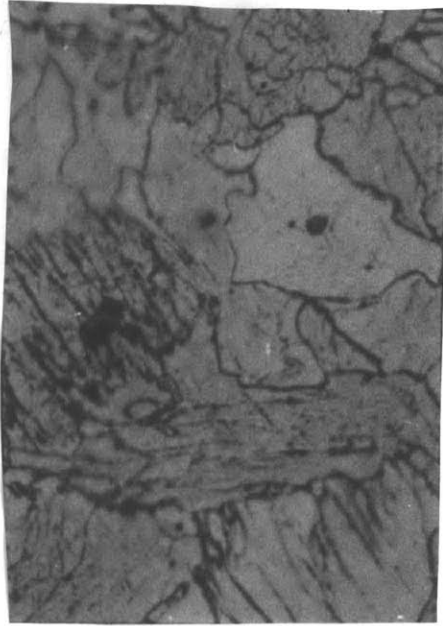


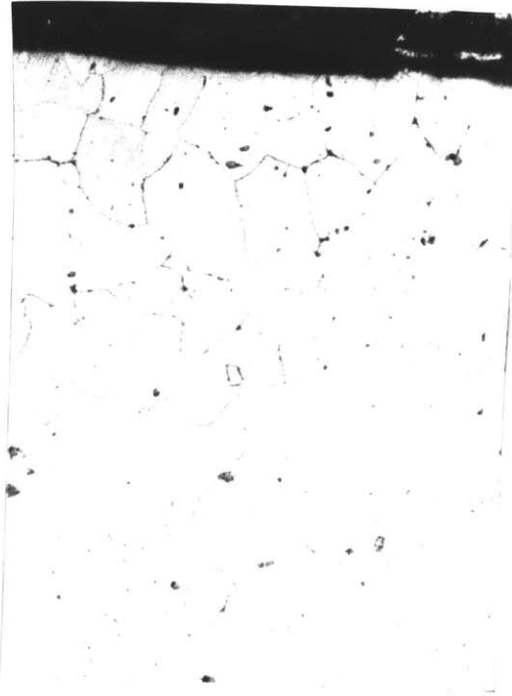
Fig. 26 - Armco iron rod
after discharge with 6
capacitors at 15 kV. 200X

The microstructure of the rods (shown in figures 25 and 26) indicates that a phase transformation took place: the grains have been completely reformed. This cannot result from applying stresses or temperature for short times unless the material has recrystallized. It is possible, however, that the transition sequence has been $\alpha \rightarrow \gamma \rightarrow \alpha$ instead of $\alpha \rightarrow \epsilon \rightarrow \gamma$. Note that the α , γ , and ϵ lattices (bcc, fcc, hcp) can be derived from one another by simple atomic displacements. These reactions can occur exceedingly fast^{7, 32} and by a martensitic mechanism.^{7, 47}

The $\alpha \rightarrow \gamma \rightarrow \alpha$ sequence seems an improbable explanation for the transformed microstructure because iron rods which were fired at slightly lower pressure levels do not show any restructuring, even in the outer regions. Figure 27 shows such a shot. Figures 28 and 29 illustrate the effects of high temperature on the end of the rod shown in figure 27. Arcing at the rod-electrode junction created sufficient heat to melt part of the copper discs. Thus, the surface shown in figure 28 was in contact with a 1000°C heat reservoir during and after the discharge, and the $\alpha \rightarrow \gamma \rightarrow \alpha$ transition sequence is expected to have occurred. Small grain size and carbon precipitation distinguish the resulting microstructure from that

of figures 26, 31 and 36.

Fig. 27 - 4mm annealed Armco rod. After 7 capacitors, 14kV
100X



The heat flow into the rod can be evaluated with the equation

$$\frac{\partial T}{\partial t} = \alpha \Delta^2 T = \frac{1}{r} \frac{\partial}{\partial r} \left(r \frac{\partial T}{\partial r} \right). \quad (10)$$

The exact solution involves the Bessel functions J_0 . In order to estimate the order of magnitude of the temperature rise, equation (10) is evaluated with the approximation.



Fig. 28 - Microstructure of rod shown in figure 27 at the electrode junction. 100X

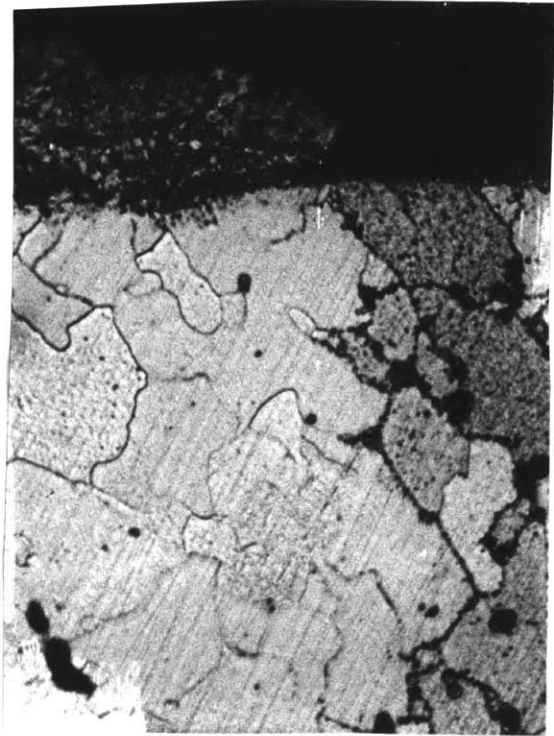


Fig. 29 - Same as figure 28. 500X

$$\frac{\Delta T}{\Delta t} \cong \bar{\alpha} \frac{\Delta T}{\Delta x^2} .$$

In this relation, $\bar{\alpha}$ is the mean thermal diffusivity of iron, about $.10 \text{ cm}^2/\text{sec}$ (ref. 49). $\Delta T \leq 5000^\circ\text{C}$; $\Delta x \approx .1 \text{ cm}$.

$$\frac{\Delta T}{\Delta t} \cong .10 \times \frac{5 \times 10^3}{10^{-2}} = 5 \times 10^4 \text{ }^\circ/\text{sec}.$$

It is apparent from the oscillographs that the discharges never last longer than about $20 \mu \text{ sec}$. In this short time, the rod cannot heat significantly. It may be possible, nevertheless, that sufficient heat is stored in the plasma to heat the rod after the current has ceased. In order to reduce the possibility of this occurring, the remainder of the experiments were carried out with the 5mm ventilating holes which had been installed for the laser studies.

Microhardness measurements were made on the rods shown in figures 25 and 26; the Vicker's hardness decreased by about 10% as a result of the discharge. This has been attributed in release of internal stresses caused by machining or inhomogeneities in the stock.

The experiments were repeated with three modifications: the iron rods were annealed, the rods were fit snugly into the BN cylinders (see fig. 4), and the 5mm ventilating holes were present. As discussed in section 5.1, one effect of these changes was to hinder the disintegration of the rods.

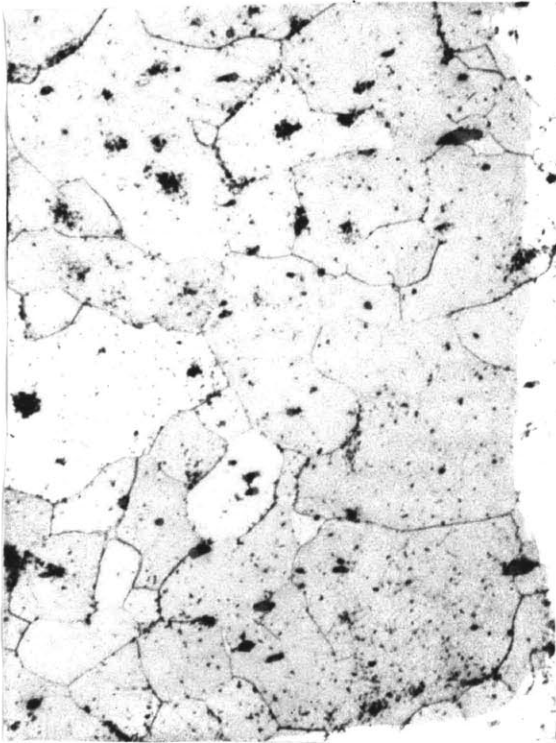


Fig. 30 - 4mm annealed iron rod.
100X

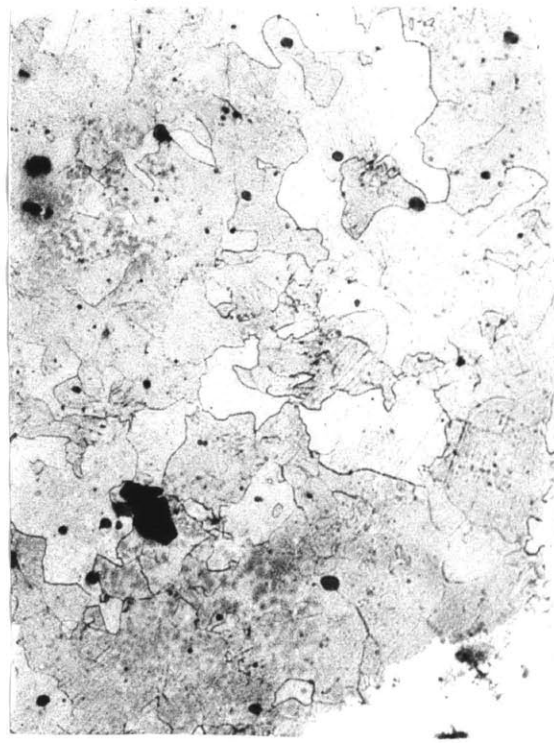


Fig. 31 - 4mm annealed rod after
discharge, 6 capacitors, 16.5 kV. 100X

Figure 30 shows an example of the annealed stock. Figure 31 shows the microstructure of the only one of the recovered rods which showed evidence of a phase transition; in this sample the disturbed grains were clearly concentrated along the axis. This is consistent with a pressure effect (as opposed to a temperature effect). Unfortunately, the sample could not be photographed with a sufficiently low power microscope to show this concentration. The micro-

hardness of the rod shown in figure 31 was about 10% higher than that of the annealed stock.

In an attempt to reduce the final temperature, rods were cooled to liquid nitrogen temperature prior to firing. Although the additional heat required to raise the iron to a high temperature was small, the experiment was simple for us to do. The main result of cooling was apparently to increase the conductivity (or increase the brittleness), for the energy required to destroy the rods was reduced.

It was clear from even casual inspection of damaged rods that destruction occurred largely at the ends; the top and bottom of the rods would frequently be broken away, and the copper electrodes near the rods were often melted. Therefore, some flanged samples, shown in figure 32, were manufactured.

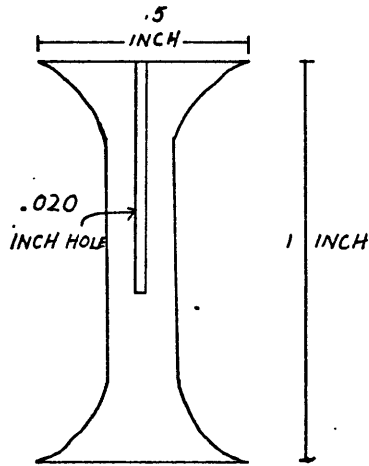


Fig. 32 - Design of flanged armco iron samples.

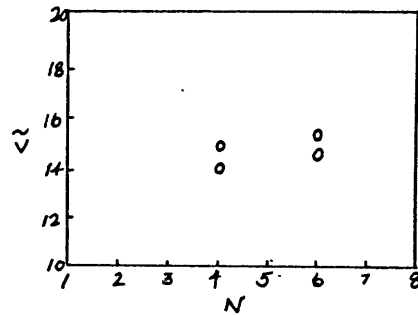


Fig. 33 - Response of flanged samples. (Symbols are explained in figure 13)

These samples were also annealed and had holes drilled in them. (The holes were filled with silver powder, and after the experiment the powder was examined for evidence of melting. The powder was fused after the experiments; however, pressure alone can fuse powder, and clear conclusions could not be drawn.)

The flanged samples were found to disintegrate at slightly lower energy levels than straight rods, as shown in figure 31. However, in complete contrast to the straight rods, these samples disappeared from the center, sometimes leaving the top and bottom flanges undamaged and the copper electrodes reusable. The lower disintegration threshold is attributed to higher current densities. Because of the lower thresholds and some prefires, the highest pressure which was obtained with these rods was with 4 capacitors at 14.6 kV. This specimen was accidentally ground too far during metallographic polishing; only the outer regions could be studied, and there was no evidence of a phase transition.

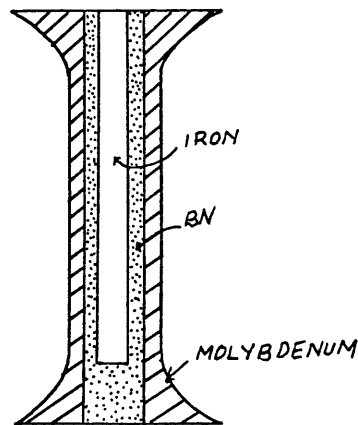


Fig. 34 - Insulated iron sample.

The latest and most sophisticated sample design employed is shown in figure 34. At present only one experiment has been carried out with this modification. The level was 18 kV and 8 capacitors; no oscilloscope record was obtained because of prefire. Even at such a high energy, the rod remained intact. Assuming a discharge time of 8μ sec, the resulting pressure was over 250 kilobars. Evidence for a phase transition was clearly present. Figures 35 and 36 show photomicrographs of the stock metal and the iron rod after the discharge. Figure 37 illustrates an increase in hardness of about 20%.

34.

Fig. 35 - Annealed stock.
75X

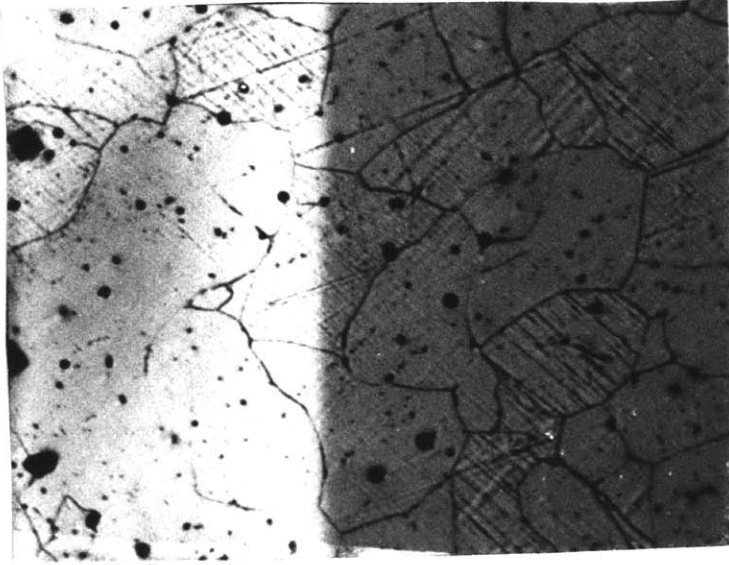
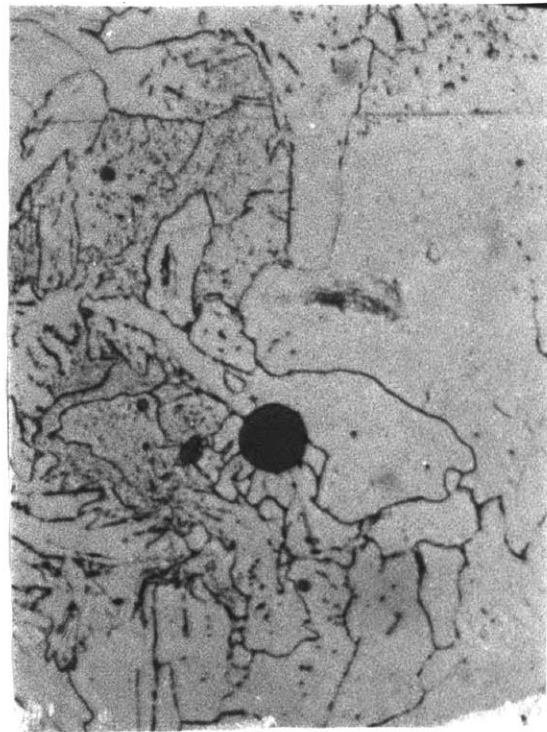
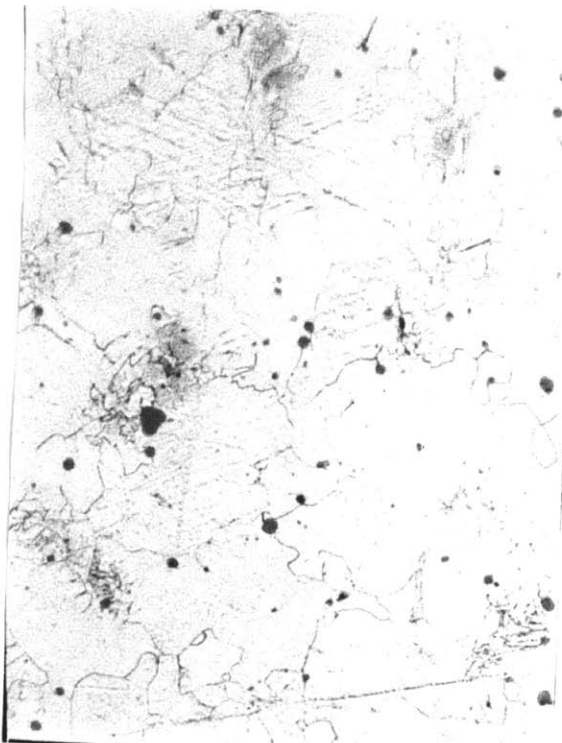
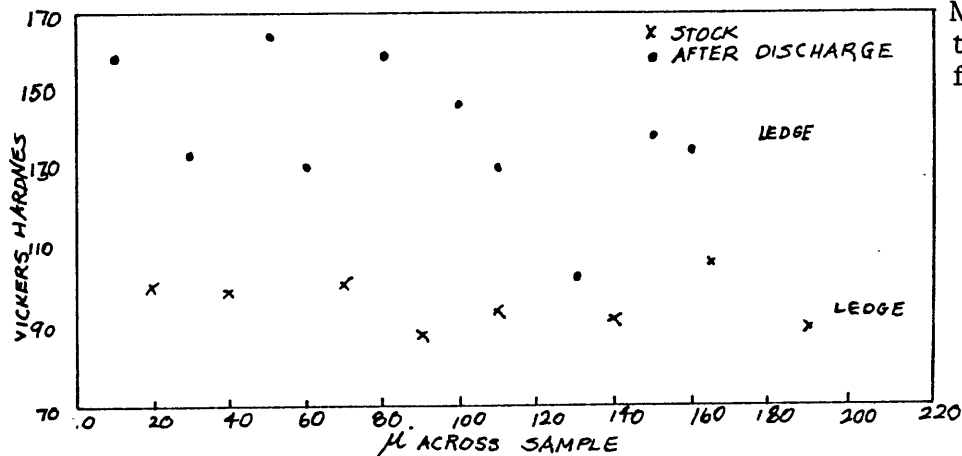


Fig. 36 - Two views of the sample shown in figure 34 after discharge with
8 capacitors, 18kV.

100X

500X





In this sample it is less likely that enough heat could have flowed into the iron rod to cause the $\alpha \rightarrow \gamma$ transition. The heat flow across the boron nitride is

$$Q \approx K \frac{\Delta T}{\Delta x} = 650 \text{ cal/cm}^2 \text{ - sec}$$

using $K = .05 \text{ cal cm}^3 / \text{sec}^\circ\text{C}$, $\Delta T = 2600^\circ\text{C}$ (corresponding to the melting point of molybdenum), and $\Delta x = .2 \text{ cm}$. The area $2\pi r l$ is 3.2 cm^2 . For iron, $\rho_s = .82 \text{ cgs}$, thus

$$\frac{\Delta T}{\Delta t} = \frac{A}{\rho_s V Q} = 7800^\circ/\text{sec}$$

Since the sample was unconfined, there was no arcing, and ventilating holes were present, there could have been no source of heat existing for longer than a few microseconds.

As a check on this analysis, two of the samples shown in figure 32 were instrumented with a chromel-alumel thermocouple in place of the iron rod. The thermocouple was connected to an oscilloscope through a relay which closed about .5 seconds after the capacitors were fired.

In the first thermocouple experiment, some of the eight capacitors pre-fired at 13 kV; those remaining were fired about 30 seconds later. Thermocouple

records taken during the firing sequence showed a rise in temperature of less than 100°C . The next shot was with eight capacitors at 16 kV. Unfortunately, a carelessly positioned shielding cable shunted part of the current, resulting in considerable damage to the mylar insulation sheets. The sample broke (probably because of the asymmetrical current distribution), and the thermocouple was destroyed.

Additional experiments with thermocouples are desirable, and will hopefully be completed soon. However, the metallographic and theoretical analyses seem sufficient to conclude that the high pressure phase of iron has been produced.

4.4 Experiments with boron nitride

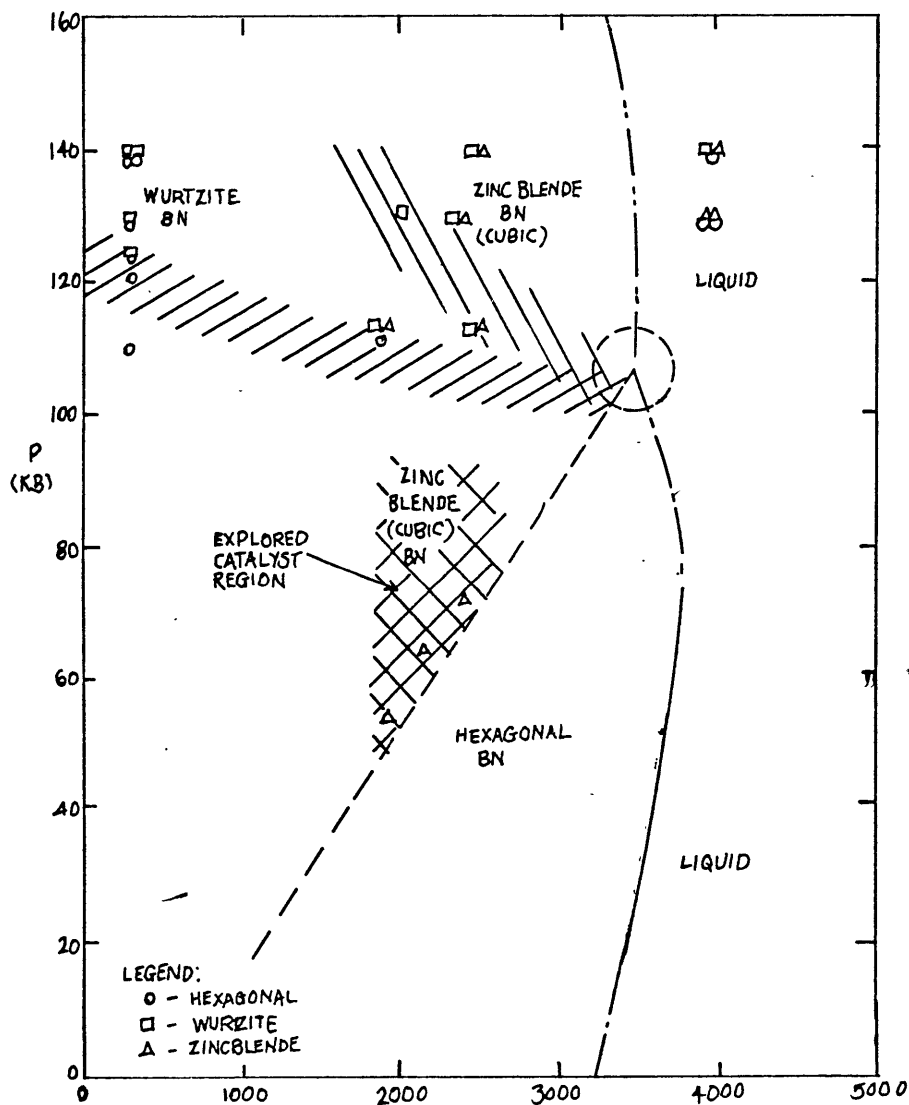
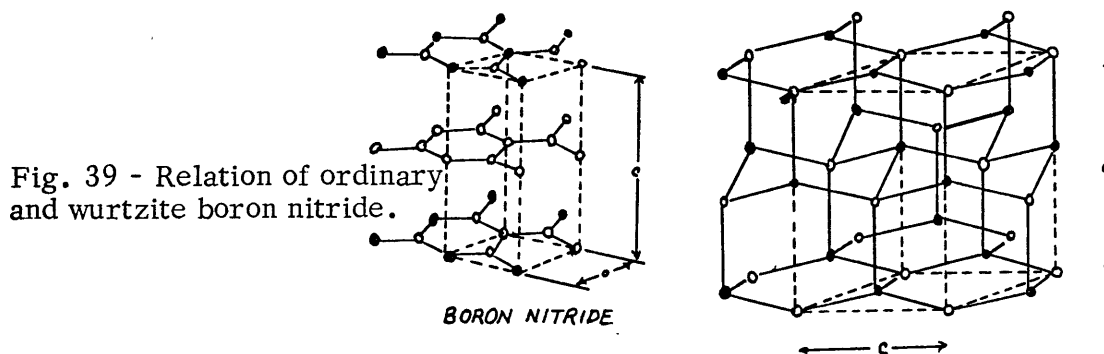


Fig. 38 - Phase diagram of boron nitride. (from Ref. 13)

The phase diagram of boron nitride, as determined in static experiments, is shown in figure 38. As marked on the diagram, ordinary hexagonal boron nitride transforms to a high pressure wurtzite structure at about 120 kilobars; figure 39 shows how these two structures are related. The cubic phase of BN is similar to the diamond phase of carbon; these substances are the two hardest materials known.⁴⁶



The high pressure polymorph has been produced in shock experiments by Al'tshuler;² he also observed that the high pressure phase did not recrystallize to the "graphite" phase when the pressure was released. Because of the rapidity of the transition, and because the high pressure form can be recovered, boron nitride was selected for experiments with our apparatus.

The first series of experiments are described in Table 3. In the table, Cu stands for rods which were electroplated with copper, ss stands for rods pressed into stainless steel tubes, pf stands for prefire (which means that no oscilloscope record was obtained). Two types of chambers were used: A = Apiezon stuffed into the guard ring around the sample, and N = nylon cylinder in place of the usual boron nitride one (see figure 4); nh stands for no 5mm holes.

Table 2 - Boron nitride experiments, first series. N, \tilde{V} , \tilde{T} have the same meaning as in equation 7. Other abbreviations are defined in the text.

#	BN dia (mm)	sleeve	chamber	N	\tilde{V}	\tilde{T}
B1	2.6	ss	A	4	16	1.5
B2	2.4	Cu	A	6	16.5	1.5
B3	2.4	Cu	A	6	16.5	1.5
B4	2.6	ss	N	7	11	pf
B5	2.6	ss	N	7	13	pf
B6	2.4	Cu	N	8	15.5	pf
B7	2.4	Cu	N	8	17	pf
B8	2.4	Cu	N	8	19.8	4

In these and subsequent experiments, the BN rods were broken but easily recognizable among the debris in the sample chamber. Fragments of the rods were ground, and Debye-Scherrer patterns were obtained. The "d" values were compared with those given by Bundy¹³ for the cubic and wurtzite forms. Only in B8 were peaks corresponding to cubic BN identifiable. However, a check of contaminants revealed that copper has the same structure and unit cell dimensions, and hence the same Debye-Scherrer pattern as cubic boron nitride. Therefore, the experiments were repeated with stringent precautions against copper contamination. Only stainless steel encased BN rods were used, and the copper electrodes were replaced with stainless steel discs. Table 3 gives the parameters:

Table 3 - Boron nitride experiments, second series. (Symbols are defined in Table 2.)

#	BN dia (mm)	sleeve	chamber	N	\tilde{V}	\tilde{T}
B9	3.5	ss	N	6	15	pf
B10	3.5	ss	N	7	17.2	6
B11	3.5	ss	N, nh	8	19.0	8
B12	3.5	ss	N	8	19.5	7

The pressures generated in samples B10, B11, and B12, using equation 7, were 185, 117, and 220 kilobars. However, the X-ray patterns showed no trace of any high pressure phase of BN in these samples. There are three alternative conclusions:

- Large overdriving or shear stresses, which are absent in our experiments, are required to transform boron nitride in short times.
- The thickness of the stainless steel cylinders inhibited pressure transmission to the rods.
- High pressures were not achieved.

Figure 39 shows the shock Hugoniot of boron nitride:

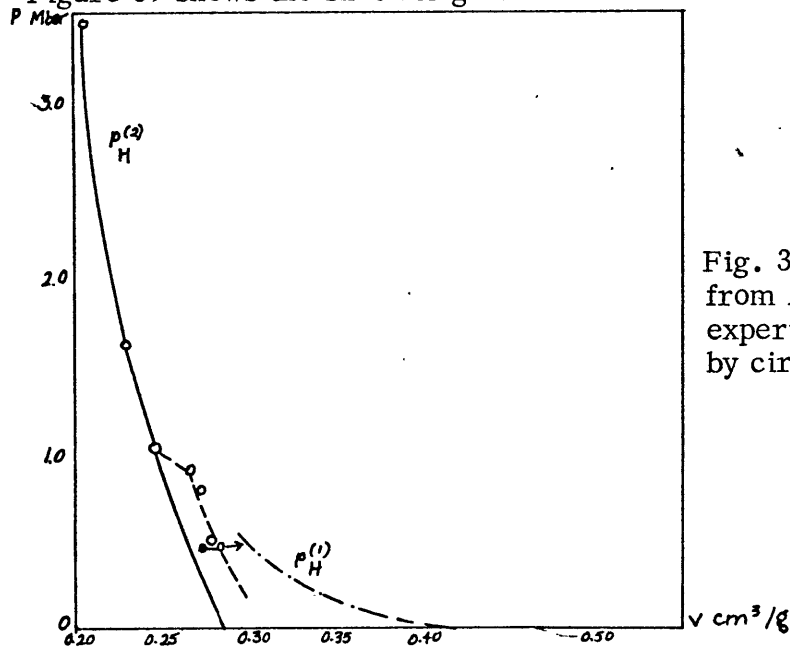


Fig. 39 - Shock hugoniot of BN, from Al'tshuler (ref. 2). The experimental points are marked by circles.

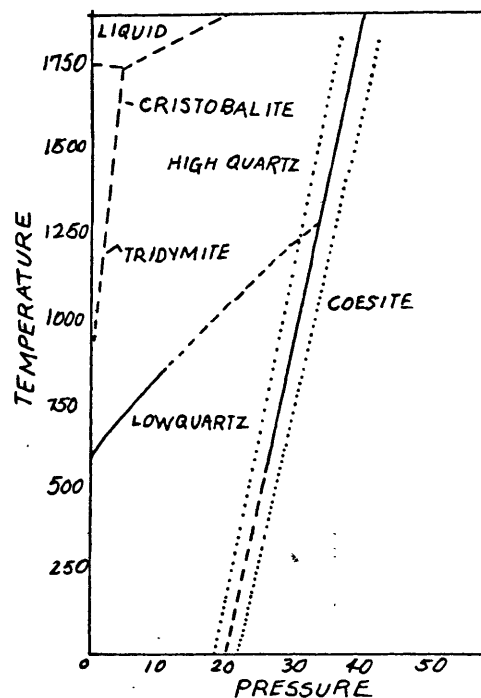
Al'tshuler interprets the region between 900 and 190 kilobars as arising from erroneous shock velocity measurements. We suggest, as an alternative explanation, that the transition to cubic boron nitride was incomplete below 900 kilobars. Similar partial transformation occurs in shocked carbon.¹

The thickness of the stainless steel tubing may considerably inhibit the inward transmission of pressure. In most of the experiments, the wall thickness was .025 inches (.63mm); this is comparable to the wavelength of the pressure pulse, travelling at the speed of sound. Acoustic mismatch, with reflection, may occur.

Although high pressure boron polymorphs have not been detected, it would be premature to conclude that the pinch pressure did not reach the predicted values. In order to clarify these results, experiments, with very thin walled tubing will be conducted in the future.

4.5 Experiments with quartz

Fig. 40 - Phase diagram of SiO_2 .
Stishovite should be added, the transition occurring at 160 kbar.⁵¹

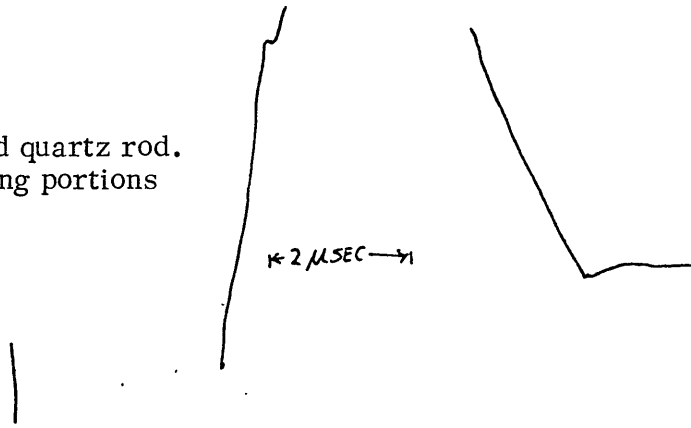


SiO_2 occurs in an unusually large number of high temperature and pressure polymorphs. Of the latter, coesite and stishovite have been found in natural meteorite craters.^{18, 19} However, only stishovite has been recovered from laboratory shock wave experiments.²¹ Since conditions in the pinch may be similar

to those in an impacting meteorite, a few experiments with used quartz rods were attempted.

One 1/8 inch diameter GE fused quartz rod was shrunk to fit into a stainless steel tube. The tube was then machined to a wall thickness of .25 mm. The rod was fired with 8 capacitors at 17.7 kV. The oscillograph is reproduced in figure 41.

Fig. 41 - Oscillograph. Fused quartz rod. 8 capacitors, 17.7 kV (Missing portions of the curve were offscale.)



A very large amount of energy was put into the sample chamber in this shot. An extraordinary amount of effort was required merely to disassemble the phenolic blocks. Although the copper rings showed no indication of arcing, they were expanded almost 1/8 inch. Outward pressure also apparently blew out the steel guard ring to 5/8 inch ID and cracked the phenolic clamp blocks. The boron nitride cylinder in the sample chamber was either compressed to half its volume or blown away. No other experiment caused such damage.

Portions of the quartz rod and boron nitride cylinder were recovered for analysis. The fragments were immersed in concentrated nitric acid in order to prevent copper contamination. Unfortunately, it was not possible to obtain Debye-Scherrer patterns until one week after the experiment had been run.

The SiO_2 pattern showed lines of ordinary BN, aluminum (from the specimen

holder), and iron. Bragg angles based on the reported spacings of α quartz,³ β quartz,³ tridymite,³ coesite,¹⁰ stishovite,⁵¹ silicon,³ and dense silicon⁷⁰ were checked against the pattern with no matches. There were four distinct peaks which could not be identified; they correspond to d values of 1.31, 1.24, 1.21, and 1.16 angstroms.

The boron nitride powder produced no recognizable lines of any known phase of boron nitride. Peaks corresponding to aluminum and iron were present again. Two weeks later some more of the boron nitride pieces were ground and analysed. This time all of the lines associated with ordinary boron nitride appeared. There was no trace of zincblende or wurtzite BN, however.

The results of this experiment are intriguing because there is no apparent explanation for them. Prior to the shot, the ground geometry of the capacitor bank had been changed, but we can see no way this could have affected the discharge. This was the only sample fired which had a conductor thickness comparable with the skin depth; perhaps some sort of resonance occurred. The absence of α quartz lines in the Debye-Scherrer pattern is not anomalous, since fused quartz has no periodicity. Wackerle found that quartz shocked above 383 kilobars became amorphous,⁵² thus it is possible that the rod was subjected to much higher pressures than anticipated. It is also possible that fine grains of transformed material escaped recovery. However, at this time, both of these hypotheses are speculation. The d values obtained have never appeared in the numerous stainless steel encased BN rods which have been analysed.

The lack of BN peaks in the powder pattern first run may be due to experimental error, since the lines were present in the quartz pattern and in the later BN pattern. However, it is difficult to imagine how a mistake could have been made.

The failure to observe traces of high-pressure quartz polymorphs can thus be explained three ways:

- a) Pressures above 380 kbars were reached, where the stable phase is amorphous.
- b) There was only time for small quantities of stishovite to form, which were not recovered.
- c) High pressures were not achieved.

The anomalous X-ray patterns could result from:

- d) Experimental error (in procedure or by contamination)
- e) Production of a new high pressure polymorph of SiO_2 , which spontaneously converts (in powder form) to α -quartz within a few weeks, at STP.

The results obtained with iron suggest that hypothesis (b) is correct. Only further experiments can distinguish between hypotheses (d) and (e).

5. CONCLUSION

The electrical pinch may have a useful role to play in high pressure research. A wide range of pressures and temperatures are theoretically obtainable. The characteristics of the compression differ from those of conventional high pressure equipment, and may be valuable in studying reaction mechanisms and temperature effects.

Our preliminary result is that the 130 kilobar transition in iron has been produced by pinch generated pressure. Although some problems remain in the interpretation of the data, we feel it is unlikely that this conclusion will be modified. The attempts to produce high pressure modifications of boron nitride and quartz have been inconclusive.

6. ACKNOWLEDGEMENTS

Recognition must be given to the late Professor Francis Bitter, for it was he who conceived of the experiment and the original low inductance circuit design. Professor Giorgio Fiocco has been very helpful with numerous suggestions on procedure. Recently, Dr. Winfield Salisbury of S.A.O. has given valuable advice on experiment design and interpretation.

7. REFERENCES

1. B. J. Adler & R. H. Christian, "Behavior of Strongly Shocked Carbon", *Phys. Ref. Letters* 7, 367-8, 1961.
2. L. V. Al'tshuler, "Peculiarities of Phase Transitions in Compression and Rarefaction Shock Waves", *Sov. Phys. JETP* 25, 260-65, 1967.
3. American Society for Testing and Materials, Powder Diffraction File.
4. D. Bancroft et. al., "Polymorphism of Iron at High Pressure," *J. Appl. Phys.* 27, 291, 1956.
5. F. D. Bennett et. al., "Correlated Electrical and Optical Measurements of Exploding Wires", *Phys. of Fluids* 5, 102-13, 1962.
6. F. D. Bennett et. al., "Resistance Changes Caused by Vaporization Waves in Exploding Wires", 65-88 in reference 23.
7. M. J. Bibby & J. G. Parr, "The Martensitic Transformation in Pure Iron", *J. Iron and Steel Inst.* 202, 100-104, 1964.
8. F. Birch, "Geophysical Application of High Pressure Research", in *Solids Under Pressure*, ed. W. Paul & D. M. Warschauer, McGraw Hill, 1963.
9. J. L. Bohn et. al., "Acceleration of Small Particles by Means of Exploding Wires", 339-352 in reference 23.
10. F. R. Boyd, "Phase Equilibria in Silicate Systems at High Pressures and Temperatures", in *Modern Very High Pressure Techniques*, ed. R. H. Wentorf, Butterworth, 1962.
11. F. R. Boyd & J. L. England, "The Quartz-Coesite Transition", *J. Geophys. Res.* 65, 749-56, 1960.
12. F. P. Bundy, "Pressure-Temperature Phase Diagram of Iron to 200 kbar, 900°C, *J. Appl. Phys.* 36, 616-20, 1965.
13. F. P. Bundy & R. H. Wentorf, "Direct Transformation of Boron Nitride to Denser Forms", *J. Chem. Phys.* 38, 1144-49, 1963.
14. W. G. Chace & H. K. Moore (eds), *Exploding Wires Volume 1*, Plenum Press, 1959.
15. W. G. Chace & H. K. Moore (eds), *Exploding Wires Volume 2*, Plenum Press, 1962.
16. W. G. Chace & H. K. Moore (eds), *Exploding Wires Volume 3*, Plenum Press, 1964.
17. *Ibid.* pp. 125-193.

18. E. C. T. Chao et. al., "First Natural Occurrence of Coesite", Science 132, 220-22, 1960.
19. E. C. T. Chao et. al., "Stishovite, SiO₂, a Very High Pressure New Mineral from Meteor Crator, Arizona:, (letter to the editor) J. Geophys. Res. 67, 419-21, 1962.
20. W. P. Deal, "Dynamic Pressure Techniques", in Modern Very High Pressure Techniques, ed. R. H. Wentorf, Butterworth, 1962.
21. P. S. DeCarli & D. J. Milton, "Stishovite: Synthesis by Shock Waves", Science, 147, 144-5, 1965.
22. D. G. Doran & R. K. Linde, "Shock Effects in Solids", Solid State Physics Vol. 19, 229-90, 1966.
23. H. G. Drickamer et. al., "X-Ray Diffraction Studies of the Lattice Parameters of Solids under Very High Pressure", Solid State Physics Vol. 19, 135-229, 1966.
24. H. G. Drickamer & A. S. Balchan, "High Pressure Optical and Electrical Measurements", in Modern Very High Pressure Techniques, ed. R. H. Wentorf, Butterworth, 1962.
25. H. D. Edelson & T. Korneff, "A Comparative Study of Exploding Wires in Air and Water", J. Appl. Phys. 37, 2166-68, 1966.
26. H. D. Edelson & T. Korneff, "Conducting Mechanisms of Exploding Wires in a Vacuum", 267-284 in reference 23.
27. A. Folkierski & R. Lathane, "Shock-Waves in a Pinched Discharge", C. R. VI Conférence Internationale sur les Phénomènes D'Ionisation dans les Gaz, 617-19, Paris, 1963.
28. C. M. Fowler et. al., "Production of Very High Magnetic Fields by Implosion", J. Appl. Phys. 31, 588-94, 1960.
29. I. M. Fyfe & R. R. Ensminger, "Explosive Wire Induced Cylindrical Waves in Solids", 257-266 in reference 23.
30. J. J. Gilvary, "Temperatures in the earth's Interior", J. Atmos. Terres. Phys. 10, 84-95, 1957.
31. R. A. Graham et. al., "Shock Wave Compression of Germanium from 20 to 140 kbar", J. Appl. Phys. 36, 3955-56, 1965.
32. P. C. Johnson et. al., "Temperature Dependence of Shock-Induced Phase Transformation in Iron", J. Appl. Phys. 33, 557-61, 1962.
33. J. Katzenstein & J. Sydor, "Exploding Wire as a Fast Dynamic Pinch", J. Appl. Phys. 33, 718-23, 1962.

34. K. H. Kelly, "High-Temperature Heat-Content, Heat-Capacity, and Entropy Data for the Elements and Inorganic Compounds", U. S. Bur. Mines #584, 1960. page 125.
35. Ibid. page 30.
36. V. S. Komelkov, "Plasma Motions in Powerful Discharges", Proc. Second U.N. Int'l Conf. on the Peaceful Uses of Atomic Energy, Vol. 31, 382-88, Geneva, 1958.
37. W. Koppendorfer, C. R. VI Conference Internationale sur les Phenomenes D'Ionisations dans les Gas, 545-48, Paris, 1963.
38. J. D. Levin & P. F. Smith, "Production of Very High Magnetic Fields by Flux Compression", Rev. Sci. Instr. 35, 542-48, 1964.
39. Metals Handbook Vol. L, 8th Edition, Amer. Soc. for Metals, 1961.
40. R. G. McQueen et. al., "Hugoniot Equation of State of Twelve Rocks", J. Geophys. Res. 72, 4999-5036, 1967.
41. C. P. Nash et. al., "Electrical and Emissive Properties of Exploded Confined Conductors", 231-246, in reference 23.
42. R. Newton, "The Status and future of high static pressure geophysical research", in Advances in High Pressure Research Vol. I, ed. R. S. Bradly, Academic Press, 1966.
43. E. A. Perez-Albuerne & H. G. Drickamer, "Effect of High Pressures on the Compressibilities of Seven Crystals Having the NaCl or CsCl Structure", J. Chem Phys. 43, 1381-85, 1965.
44. D. J. Rose & M. Clark, Plasmas and Controlled Nuclear Fusion, chapter 14, M.I.T. Press, 1961.
45. G. Schenk & J. G. Linhart, "Compression of Magnetic Fields by Exploding Foils", 223-230 in reference 23.
46. C. B. Slawson, article on diamonds, McGraw Hill Encyclopedia of Science and Technology, Vol. 4, 97-101, 1960.
47. C. S. Smith, "Metallographic Studies of Metals after Explosive Shock", Trans. Met. Soc. AIME, 574-88, Oct. 1958.
48. C. S. Smith & C. M. Fowler, "Further Metallographic Studies of Metals after Explosive Shock", Response of Metals to High Velocity Deformation, ed. P. G. Shewman & V. F. Zackay, New York, 1961.
49. H. R. Shanks et. al., "Thermal Properties of Armco Iron", J. Appl. Phys. 38, 2805-92, 1967.
50. L. Spitzer, "Controlled Nuclear Fusion Research, September 1965: Review of Experimental Results", Plasma Physics and Controlled Fusion conf. proc. IAEA, Vienna, 1966.

51. S. M. Stishov & S. V. Popova, НОВАЯ ПЛОТНАЯ МОДУЛЬ КАУСАЯ
ОКНЦН КРЕМННЯ, *Geokhimiia*, 837-39, 1961.
52. J. Wackerle, "Shock-Wave Compression of Quartz", *J. Appl. Phys.* 33,
922-37, 1962.
53. R. H. Wentorf, & J. S. Kasper, "Two New Forms of Silicon", *Science*
139, 338-9, 1963.
54. P. J. Wyllie, "Applications of High Pressure Studies to the Earth Sciences",
in High Pressure Physics and Chemistry Vol. 1, ed. R. S. Bradley, Academic
Press, 1966.